Evaluation of a Spline Reconstruction Technique: Comparison with FBP, MLEM and OSEM

George A. Kastis, Anastasios Gaitanis, Yolanda Fernandez, George Kontaxakis, Athanassios S. Fokas

Abstract–An efficient, two-dimensional, analytic, Spline Reconstruction Technique (SRT) has been presented earlier in the literature. This technique involves the Hilbert transform of the sinogram which is approximated in terms of natural cubic splines. The aim of this study is to evaluate the SRT algorithm using Monte-Carlo simulated sinograms and real PET data, in comparison with three commonly used reconstruction algorithms: FBP, MLEM and OSEM.

For the simulation studies, a digital Hoffman phantom, a NEMA-like and a Derenzo phantom were employed, and Monte Carlo methods were used for the simulation of the activity distribution in the source and the resulting generation of positron-electron annihilations. No noise, scatter and absorption conditions were assumed. The phantoms were generated with different image activities. The relevant modeled system was a single-ring tomograph with 234 scintillation crystals. Image grids with an image size of 128 × 128 pixels were employed. For the studies of real data, PET sinograms of an FDG injected mouse and a NEMA and Derenzo phantom were acquired from an ARGUS-CT small animal PET/CT system. Both the simulated and real sinograms were reconstructed using the SRT algorithm and the reconstructed images were compared to those of FBP, MLEM and OSEM. The contrast and SNR were calculated for the simulated NEMA-like and Hofmann phantom by drawing ROIs within the images.

Our results indicate that SRT and FBP give reconstructed images of comparable quality with respect to the number of counts. Striking artifacts become worse at lower total counts for both methods. SRT reconstructed images exhibit higher SNR in comparison with FBP and, in some cases, in comparison with MLEM and OSEM. SRT reconstructed images exhibit higher contrast over FBP but not over MLEM and OSEM. The reconstruction time for SRT was about 20 sec per slice, hence SRT is faster than MLEM and OSEM (for high activity images), but slower than FBP. In conclusion, SRT is a linear algorithm which can serve as a good alternative to FBP, providing images with higher contrast and SNR values. Furthermore, it has the crucial advantage that it can accommodate complicated detector geometries.

I. INTRODUCTION

An analytic, Spline Reconstruction Technique (SRT) was introduced in [1]. The SRT is a linear, 2D reconstruction algorithm based on an analytic formula of the inverse Radon transform [2]. This analytic formula involves the Hilbert transform of the sinogram which is approximated in terms of natural cubic splines. The algorithm involves the numerical implementation of the analytic formula.

The aim of this study is to evaluate the SRT algorithm using Monte-Carlo simulated phantoms as well as real PET data, in comparison with three commonly used reconstruction algorithms: filtered back-projection (FBP), maximum likelihood-expectation maximization (MLEM) and ordered subsets-expectation maximization (OSEM).

II. MATERIALS AND METHODS

A. Spline Reconstruction Technique (SRT)

The SRT algorithm is based on the inversion of the Radon Transform given by the formula [2]

$$f(x_1, x_2) = -\frac{1}{4\pi^2} \int_0^{2\pi} \frac{\partial h(\rho, \theta)}{\partial \rho} d\theta , \qquad (1)$$

where $h(\rho, \theta)$ is the Hilbert Transform of the data (sinogram) given by the following principal value integral:

$$h(\rho, \theta) = PV \int_{-\infty}^{\infty} \frac{\hat{f}(\rho', \theta)}{\rho' - \rho} d\rho' . \qquad (2)$$

In each interval between $[\rho_t, \rho_{t+1}]$, $\hat{f}(\rho, \theta)$ is approximated by a cubic spline in ρ, and this yields an analytic formula for $\dfrac{\partial h(\rho, \theta)}{\partial \rho}$. The SRT algorithm is based on the numerical evaluation of the integral of this expression. The analytic derivation of the formulae involved in the SRT algorithm can be found in [1].

G. A. Kastis is with the Research Center of Pure and Applied Mathematics of the Academy of Athens, Soranou Efessiou 4, Athens 11527, Greece (telephone: +30-210-659-7159, e-mail: gkastis@academyofathens.gr).

A. Gaitanis is with the Biomedical Research Foundation of the Academy of Athens (BRFAA), Soranou Efessiou 4, Athens 11527, Greece (e-mail: agaitanis@bioacademy.gr).

Y. Fernandez is with the Centre d'Imatge Molecular Experimental (CIME), CETIR Centre Medic, Barcelona, Spain (e-mail: yfernandez @cetir.es).

G. Kontaxakis is with Universidad Politécnica de Madrid, E.T.S.I. Telecomunicación, Dpto. Ingeniería Electrónica, 28040 Madrid, Spain (email: gkont@die.upm.es) and with Biomedical Research Networking Center in Bioengineering, Biomaterials and Nanomedicine (CIBER-BBN), Madrid, Spain.

A. S. Fokas is with the Department of Applied Mathematics and Theoretical Physics, University of Cambridge, Cambridge, CB30WA, UK (e-mail: T.Fokas@damtp.cam.ac.uk) and with the Research Center of Pure and Applied Mathematics of the Academy of Athens, Soranou Efessiou 4, Athens 11527, Greece.

B. Simulation Studies

We have modeled a single-ring tomograph with 234 scintillation crystals on the ring. The detector's width is 7.36 mm and the size of field-of-view (FOV) is 200×200 mm^2. The detector ring radius is 150 mm and the total number of detector tubes is 8128. We have employed image grids with a size of 128×128 pixels (pixel side = 1.56 mm) and have used Monte Carlo methods for the simulation of the activity distribution in the source and the resulting generation of positron-electron annihilations. No noise, scatter and absorption conditions were assumed.

In order to evaluate the performance of SRT algorithm, a slice of the 3D Hoffman phantom, a NEMA-like phantom, and a Derenzo phantom were employed. The value in each image pixel is given by the activity distribution in the area covered by this pixel. A corresponding number of gamma-ray pairs were generated using Monte Carlo methods for each pixel. Activity distributions of 1, 2, 4 and 8 million counts were simulated for all three test phantoms. The generated detector-pair data were reconstructed using MLEM [3] and OSEM [4] with 4 subsets. The iteration process of the MLEM and OSEM reconstructions was stopped when the normalized root mean squared deviation (NRMSD) reached its minimum value [5]. Prior to FBP and SRT reconstruction, the detector-pair data for each phantom were rebinned in order to generate parallel beam sinograms. These sinograms were then reconstructed using FBP supplemented with Hann filter. The same sinograms were reconstructed using SRT. A 2D Hann filter was also applied to the SRT reconstructed images post reconstruction. All reconstructions where executed on an Intel® Core™ i5 Processor and 4GB RAM. The reconstruction code for MLEM and OSEM was written on C programming language, whereas the FBP and SRT codes were written in FORTRAN.

C. Imaging System

All image acquisitions were performed using the ARGUS-CT small animal PET/CT system (SEDECAL, S.A., Madrid, Spain). The PET tomograph of this scanner is identical to the eXplore VISTA system and is described elsewhere [6]. Briefly, it consists of 36 detector modules arranged in two rings of 18 modules. Each module is composed of a 13×13 dual layer phoswich array of LYSO (front) and GSO (back) detectors. The CT system uses flat panel CMOS technology with a micro-columnar CsI scintillator plate and a microfocus X-ray source.

D. Phantom Studies

A phantom, made in accordance to the specifications of the NEMA NU4-2008 quality phantom [7], was filled with 16.3 MBq of ^{18}F and scanned for 30 min, followed by a CT scan. The in-house Derenzo phantom shown in Fig. 1 was imaged, in order to test the resolution limitations of the algorithms. This phantom is composed of 31 micro capillaries (72 mm length, 6.6 µl, Hirschmann Laborgeräte, Germany) arranged in six different sectors (Fig. 1). The capillaries were separated
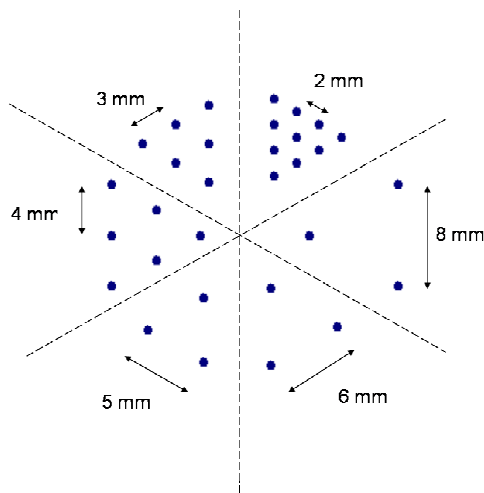
Fig. 1 In-house Derenzo phantom. The capillary holes were separated by 2, 3, 4, 5, 6 and 8 mm, respectively.

TABLE I. NUMBER OF ITERATIONS FOR MLEM AND OSEM

Image/Algorithm	1M	2M	4M	8M
NEMA/MLEM	19	21	22	24
Derenzo/MLEM	25	29	33	37
Hoffman/MLEM	75	99	130	151
NEMA/OSEM	5	6	6	7
Derenzo/OSEM	7	8	9	10
Hoffman/OSEM	29	37	31	37

by 2, 3, 4, 5, 6 and 8 mm, respectively, and no material was between them. The phantom was filled with 5.6 MBq of ^{18}F and then a 60 min PET and a CT study were performed with the entire phantom within the field of view.

E. Mouse Study

A one-year-old C57BL/6JOlaHsd male mouse (Harlan Interfauna Ibérica, S.L., Sant Feliu de Codines, Spain) was imaged. The animal was kept under standard environmental conditions and had free access to food and water before the study. A 15.8 MBq FDG dose was injected to the conscious mouse intraperitoneally; after 90 min, the animal was anesthetized with isoflurane (induction, 4 % isoflurane, 1 l/min oxygen; maintenance, 1.5% isoflurane, 3 l/min oxygen) and a PET-CT acquisition was performed (PET, 40 min).

F. Image Quality Metrics

The contrast (CR) and the signal-to-noise ratio (SNR) were employed as measures of merit for comparing the reconstructed images obtained from the Monte-Carlo simulated sinograms. The SNR and CR are given by the following expressions:

$$CR = \frac{R - B}{B}, \qquad (3)$$

where R and B are the mean activities of the region-of-interest and its background respectively:
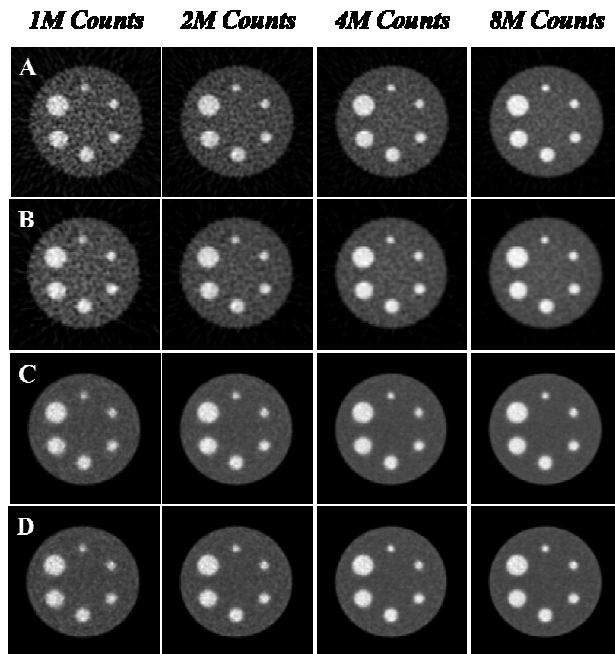
Fig. 2 Reconstructed images of a NEMA-like phantom with 1, 2, 4 and 8 million counts using A) SRT followed by a 2D Hann filter, B) FBP with a Hann filter, C) MLEM and D) OSEM. The sinograms were generated using Monte-Carlo simulation (noiseless data).
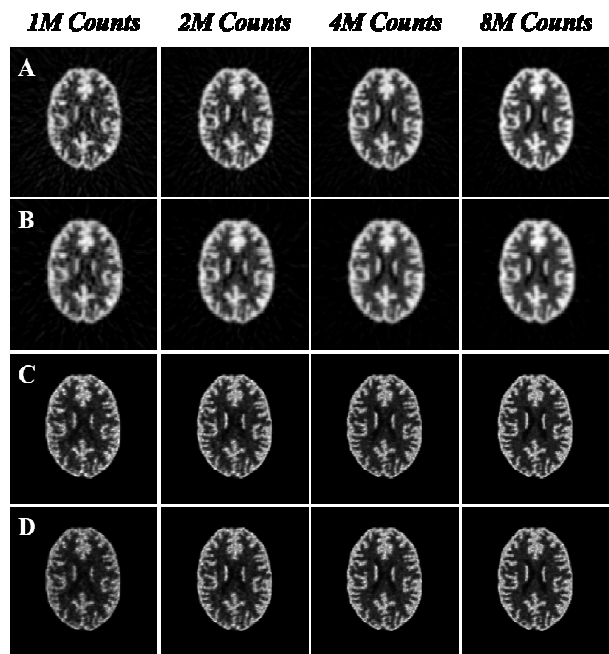
Fig. 4 Reconstructed images of a Hoffman phantom with 1, 2, 4 and 8 million counts using A) SRT followed by a 2D Hann filter, B) FBP with a Hann filter, C) MLEM and D) OSEM. The sinograms were generated using Monte-Carlo simulation (noiseless data).

$$SNR = \frac{CR}{(\sigma_B / \mu_B)}, \qquad (4)$$

where σ_B and μ_B are the standard deviation and mean of the background, respectively.

III. RESULTS

The reconstruction time for SRT was about 20 sec per sinogram (FORTRAN on Intel® Core™ i5 Processor and 4GB RAM). The reconstruction time depends on the size of the sinogram but is independent on the number of counts in the image. The execution time for FBP was about 1 sec and that of OSEM and MLEM varied depending on the number of counts in the image and the number of iterations. The number of iterations for the various simulated phantoms for MLEM and OSEM are given in Table 1. Therefore, SRT is for most cases (depending on the number of iterations) faster than MLEM and OSEM but slower than FBP.

Comparisons between SRT, FBP, MLEM, and OSEM reconstructed images, with respect to the number of counts in the initial image, are shown in Figures 2-4 for a NEMA-like, a Derenzo and a Hoffman phantom, respectively. Both SRT and FBP appear to give comparable images with respect to the number of counts. Small striking artifacts are present in both reconstruction techniques which become more evident at the lowest image activity. As expected, no artifacts are present at the MLEM and OSEM reconstructions.

Fig. 3 Reconstructed images of a Derenzo phantom with 1, 2, 4 and 8 million counts using A) SRT followed by a 2D Hann filter, B) FBP with a Hann filter, C) MLEM and D) OSEM. The sinograms were generated using Monte-Carlo simulation (noiseless data).
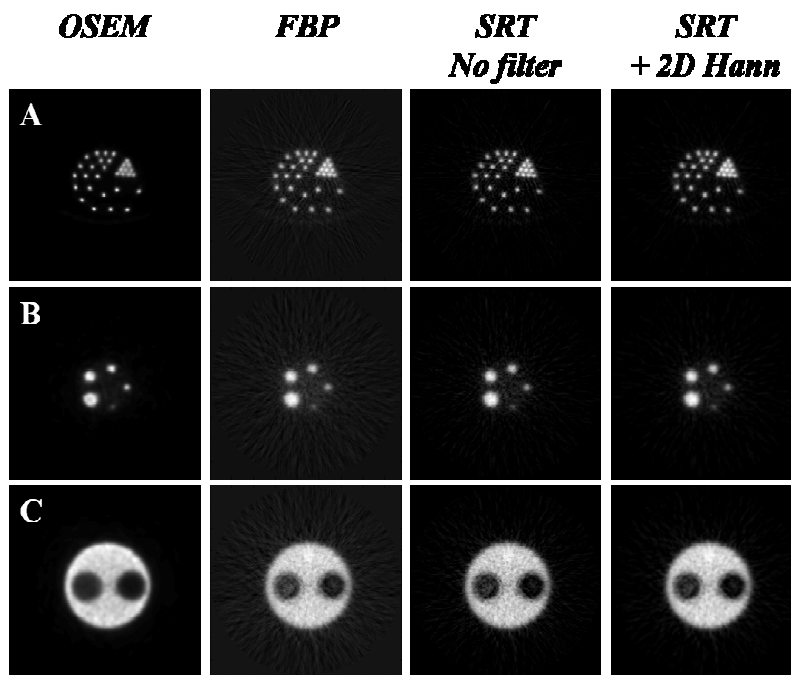
Fig. 5 Real PET data acquired by the ARGUS PET/CT scanner. (A) Reconstructions of a Derenzo phantom, and (B) and (C) two slices of a NEMA phantom.
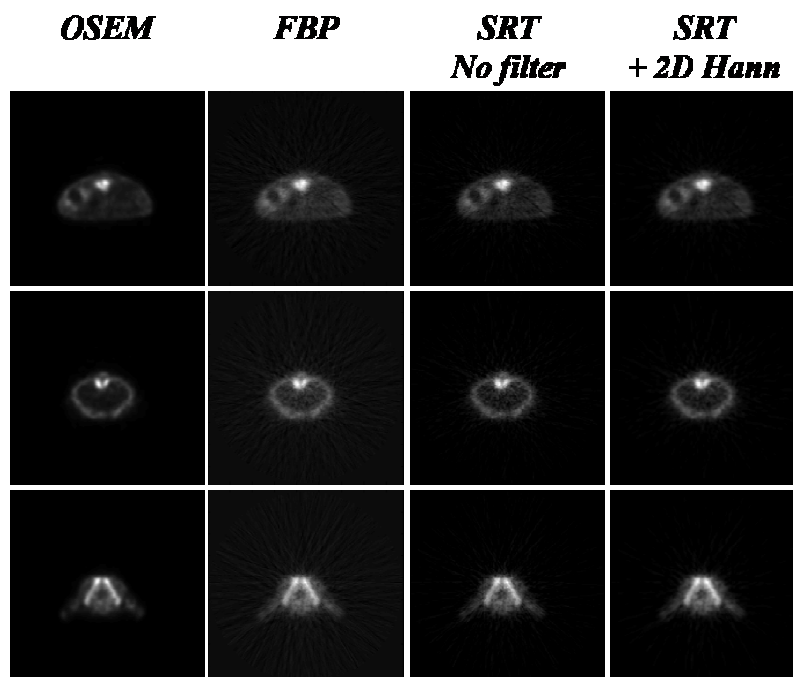
Fig. 6 Three different slices of an FDG mouse scan acquired by the ARGUS PET/CT small-animal scanner by Sedecal, Spain. Comparison between the different reconstruction methods.
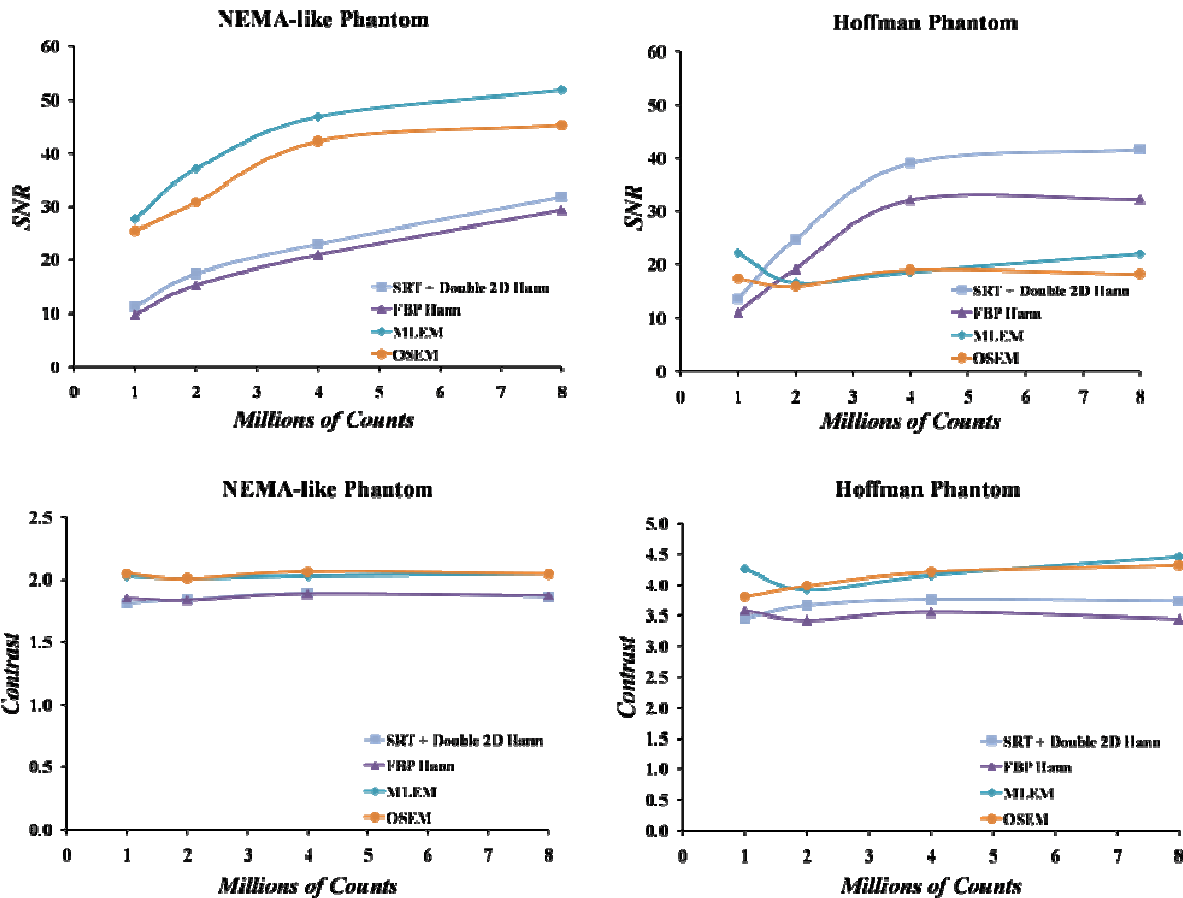
Fig. 7 SNR and contrast comparisons for the various reconstruction methods for the NEMA-like and Hoffman Monte-Carlo simulated phantoms.

Reconstructions of the real PET data acquired by the ARGUS PET/CT system indicate that the SRT algorithm provides good quality images even without any filtering (Fig. 5 and Fig. 6). All circular sources of the NEMA phantom are clearly resolved. Furthermore, the final reconstructed image appears to be of higher contrast than that of FBP. In the case of the Derenzo phantom, even the smallest capillaries, separated by 2 mm, are clearly resolved with higher contrast than FBP and OSEM.

The above subjective observations are consistent with our calculation of SNR for the NEMA-like and Hoffman simulated phantoms, which show that the SRT reconstructed images exhibit higher SNR in comparison with FBP and, in some cases, in comparison with MLEM and OSEM (Fig. 7). On the other hand, SRT reconstructed images demonstrated higher contrast only over FBP but not over MLEM and OSEM. In all algorithms, the SNR increased as the image activity increased, whereas the contrast remained about the same.

IV. DISCUSSION

In this paper we have evaluated the SRT algorithm in comparison to FBP, MLEM and OSEM using Monte-Carlo simulated phantoms and real PET data.

Our evaluation of SNR and contrast in the simulated data, shows that the SRT algorithm provides a good alternative to FBP providing images with higher contrast and SNR values. A crucial advantage of SRT is that it does not require a sinogram with evenly spaced angles and detectors, and that it can accommodate complicated detector geometries.

The problems of optimizing the reconstruction time for SRT and minimizing the striking artifacts are under consideration. More work is needed for the evaluation of SRT is needed using image quality metrics for real data.

REFERENCES

[1] Fokas A.S., Iserles A., and Marinakis V., "Reconstruction algorithm for single photon emission computed tomography and its numerical implementation," J R Soc Interface, vol 3, no 6, pp 45-54, 2006.

[2] Fokas A.S. and Novikov R.G., "Discrete analogues of $\overline{\partial}$-equations and of Radon transform," CR Acad Sci Paris Ser I Math, vol, 313, no 2, pp. 75-80, 1991.

[3] L.A. Shepp, Y.Vardi, "Maximum Likelihood Reconstruction for Emission Tomography," *IEEE Trans. Med. Imag.*, Vol. 1, nº 2: 113-121, 1982.

[4] M. Hudson, R. S. Larkin, "Accelerated Image Reconstruction using Ordered Subsets of Projection Data," *IEEE Trans. Med. Imag.* 13: 601-609, 1994.

[5] Gaitanis A., Kontaxakis G., Spyrou G., Panayiotakis G., Tzanakos G., "PET image reconstruction: A stopping rule for the MLEM algorithm based on properties of the updating coefficients". *Comput Med Imaging Graph*, vol 34, no2, pp 131-41, 2010.

[6] Wang Y, Seidel J, Tsui BM, Vaquero JJ, Pomper MG. Performance evaluation of the GE healthcare eXplore VISTA dual-ring small-animal PET scanner. J Nucl Med 2006;47:1891-1900.

[7] National Electrical Manufacturers Association. Performance measurements of small animal positron emission tomographs. NEMA standards publication NU 4-2008. Rosslyn, VA: National Electrical Manufacturers Association; 2008.